american physiological society

JNP JOURNAL OF NEUROPHYSIOLOGY

J Neurophysiol 131: 709–722, 2024.
First published March 13, 2024; doi:10.1152/jn.00285.2023

RESEARCH ARTICLE

Neural Circuits

Differential clustering of visual and choice- and saccade-related activity in macaque V3A and CIP

Zikang Zhu,[1]* Byounghoon Kim,[1]* Raymond Doudlah,[1] Ting-Yu Chang,[2] and Ari Rosenberg[1]

[1]*Department of Neuroscience, School of Medicine and Public Health, University of Wisconsin–Madison, Madison, Wisconsin, United States and* [2]*School of Medicine, National Defense Medical Center, Taipei, Taiwan*

Abstract

Neurons in sensory and motor cortices tend to aggregate in clusters with similar functional properties. Within the primate dorsal ("where") pathway, an important interface between three-dimensional (3-D) visual processing and motor-related functions consists of two hierarchically organized areas: V3A and the caudal intraparietal (CIP) area. In these areas, 3-D visual information, choice-related activity, and saccade-related activity converge, often at the single-neuron level. Characterizing the clustering of functional properties in areas with mixed selectivity, such as these, may help reveal organizational principles that support sensorimotor transformations. Here we quantified the clustering of visual feature selectivity, choice-related activity, and saccade-related activity by performing correlational and parametric comparisons of the responses of well-isolated, simultaneously recorded neurons in macaque monkeys. Each functional domain showed statistically significant clustering in both areas. However, there were also domain-specific differences in the strength of clustering across the areas. Visual feature selectivity and saccade-related activity were more strongly clustered in V3A than in CIP. In contrast, choice-related activity was more strongly clustered in CIP than in V3A. These differences in clustering may reflect the areas' roles in sensorimotor processing. Stronger clustering of visual and saccade-related activity in V3A may reflect a greater role in within-domain processing, as opposed to cross-domain synthesis. In contrast, stronger clustering of choice-related activity in CIP may reflect a greater role in synthesizing information across functional domains to bridge perception and action.

NEW & NOTEWORTHY The occipital and parietal cortices of macaque monkeys are bridged by hierarchically organized areas V3A and CIP. These areas support 3-D visual transformations, carry choice-related activity during 3-D perceptual tasks, and possess saccade-related activity. This study quantifies the functional clustering of neuronal response properties within V3A and CIP for each of these domains. The findings reveal domain-specific cross-area differences in clustering that may reflect the areas' roles in sensorimotor processing.

choice signals; neuronal clustering; oculomotor; sensorimotor; vision

INTRODUCTION

The anatomical clustering of neurons with similar functional properties is thought to support efficient neural computation through the optimization of axonal wiring (1–7). Such organization, referred to as functional clustering, is widely observed in sensory and motor cortex. For instance, primary visual cortex shows clustering of orientation selectivity (8), posterior inferior temporal cortex shows clustering of color selectivity (9), and primary motor cortex shows clustering of arm reach directions (10). Whether such clustering occurs within posterior parietal cortex (PPC), which supports integrative and sensorimotor functions (11, 12), has been less explored. Notably, PPC neurons are often selective for multiple sensory modalities and/or effectors (13–18), which may support high-dimensional representations that enable diverse and flexible behavioral repertoires (19–21). This mixed selectivity may conceivably influence functional clustering. Previous work revealed clustering of visual and vestibular self-motion cues as well as choice-related activity in the ventral intraparietal area, but whether mixed selectivity moderated that clustering was not tested (22, 23). Characterizing the

*Z. Zhu and B. Kim contributed equally to this work.
Correspondence: A. Rosenberg (ari.rosenberg@wisc.edu).
Submitted 26 July 2023 / Revised 1 March 2024 / Accepted 4 March 2024

0022-3077/24 Copyright © 2024 The Authors. Licensed under Creative Commons Attribution CC-BY 4.0.
Published by the American Physiological Society.

Downloaded from journals.physiology.org/journal/jn (076.255.028.190) on April 10, 2024.

clustering of neuronal response properties in PPC and how this relates to mixed selectivity may help reveal organizational principles that constrain the implementation of sensorimotor transformations. To this end, the present study quantified and contrasted the clustering of visual feature selectivity, choice-related activity, and saccade-related activity in area V3A and the caudal intraparietal (CIP) area of macaque monkeys.

Areas V3A and CIP are hierarchically organized neighboring brain regions that bridge visual and parietal cortex (24). Area V3A receives direct input from V1 and V2 (25, 26) and projects to CIP (27). The areas are implicated in the transformation of retinal images into three-dimensional (3-D) representations of object pose (position and orientation) and carry choice-related activity during 3-D visual discrimination tasks (28–36). Both areas contain neurons whose visual responses are modulated by extraretinal signals (37–42). Saccade-related activity predicting the direction and timing of eye movements is similarly prevalent in the two areas but begins earlier in V3A (35, 36). Neurons in both areas also form sensorimotor associations between their visual and saccade direction preferences, which are stronger in CIP. These associations may facilitate goal-directed behaviors through CIP's downstream projections to oculomotor and prehensile areas (27, 43–46).

To assess functional clustering, we compared the response properties of pairs of well-isolated single neurons simultaneously recorded with tetrodes. Visual feature selectivity, choice-related activity, and saccade-related activity clustered in both areas. However, there were also domain-specific, cross-area differences in the strength of clustering. Visual selectivity, which was measured by presenting planar surfaces at different 3-D poses, was more strongly clustered in V3A. In contrast, choice-related activity measured during a 3-D orientation discrimination task (47) was more strongly clustered in CIP. Intriguingly, saccade-related activity measured during a visually guided saccade task (48, 49) was more strongly clustered in V3A. The strength of clustering had little to no dependence on whether the neurons showed mixed selectivity. Given that functional clustering is thought to facilitate computations within the clustered feature space, these findings are consistent with V3A having a stronger role in the within-domain processing of visual and saccade-related signals. They are further consistent with CIP having a stronger role in the cross-domain synthesis of sensory and oculomotor signals. The differential clustering of visual and choice- and saccade-related activity in V3A and CIP may reflect the areas' functional contributions to sensorimotor processing.

MATERIALS AND METHODS

Animal Preparation

As previously described in detail, the experiments were performed with three male rhesus monkeys (*Macaca mulatta*) (35, 36). Briefly, the monkeys were implanted with a Delrin ring for head restraint and a removable recording grid for guiding electrodes. After recovery, they were trained to sit in a primate chair with head restraint and to fixate visual targets within 2° version and 1° vergence windows for liquid rewards. All procedures followed the National Institutes of Health *Guide for the Care and Use of Laboratory Animals* and were approved by the Institutional Animal Care and Use Committee (IACUC) at the University of Wisconsin–Madison.

Experimental Control and Stimulus Presentation

Experimental control was performed with REC-GUI software (RRID:SCR_019008) (50). Stimuli were rendered with Psychtoolbox 3 (MATLAB R2016b; NVIDIA GeForce GTX 970) and rear projected onto a polarization preserving screen (Stewart Film Screen, Inc.) with a DLP LED projector (PROPixx; VPixx Technologies, Inc.). The pixel resolution was 1,280 × 720 (70° × 43° of visual angle), and the frame rate was 240 Hz (120 Hz/eye). The screen distance was 57 cm. A circular polarizer and polarized glasses were used for stereoscopic presentation. A phototransistor circuit was used to align neuronal responses to the stimulus onset. Eye tracking was performed optically at 1 kHz (EyeLink 1000 Plus; SR Research).

Visual Stimuli

The visual stimuli were planar surfaces defined by 250 nonoverlapping dots uniformly distributed across the plane in world coordinates. The planes were 20° in diameter and presented at screen center. The dots were rendered with stereoscopic and perspective cues. Orientation was parameterized as slant and tilt (32, 51). All combinations of four slants (15° to 60°, 15° steps) and eight tilts (0° to 315°, 45° steps) plus the frontoparallel plane (slant = 0°, tilt undefined) were presented. Each orientation was presented at four distances (37, 57, 97, and 137 cm). The fixation target was always at screen distance (57 cm).

Behavioral Tasks

Tilt discrimination task.

The monkeys performed an eight-alternative forced-choice tilt discrimination task during the presentation of the planar surfaces (47). On each trial, fixation was held on a target at the center of the screen for 300 ms. A plane then appeared for 1,000 ms while fixation remained on the target. The fixation target and plane then disappeared, and eight choice targets corresponding to the eight tilts appeared (polar angles: 0° to 315°, 45° steps; 11° eccentricity). A saccade was made to the target at the side of the plane perceived as nearest (e.g., the left target for a left-near plane). A liquid reward was given for correct responses. Responses to frontoparallel planes (task ambiguous) were pseudorandomly rewarded.

Visually guided saccade task.

The monkeys also performed a visually guided saccade task (48, 49). On each trial, fixation was held on a target at the center of the screen for 1,300 ms. The fixation target then disappeared, and a saccade target appeared at one of eight locations matching the choice target locations in the tilt discrimination task. A saccade to that target was made in exchange for a liquid reward.

Trials of the two tasks were interleaved. If fixation was prematurely broken or a response was not made within 500 ms of the choice/saccade targets appearing, the trial was aborted and reshuffled into the remaining trials.

Downloaded from journals.physiology.org/journal/jn (076.255.028.190) on April 10, 2024.

Neuronal Recordings

The areas were identified based on magnetic resonance imaging scans, gray/white matter transitions, and functional properties (32–36). A total of 91 V3A and 53 CIP recording sessions were performed with linear array probes with either four or eight tetrodes separated by 300 μm (NeuroNexus, Inc.). Neuronal signals were sampled at 30 kHz (Scout Processor; Ripple, Inc.). Electrodes within a tetrode were separated by 25 μm and arranged in a diamond pattern. Because the amplitude of a recorded action potential depends on the distance between the neuron and each contact, tetrodes provide more distinct waveforms for distinguishing between neurons (52). Spike sorting was performed offline with the KlustaKwik semiautomatic clustering algorithm in MClust-4.0 followed by manual refinement based on waveform profile, stability, and refractory period violations with Offline Sorter (Plexon, Inc.). Only well-isolated single neurons verified by at least two authors (V3A: $N = 692$; CIP: $N = 437$) were included.

Data Analyses

The visual feature selectivity, choice-related activity, and saccade-related activity of the V3A and CIP neurons analyzed here have been extensively compared (35, 36). As such, the present analyses test for functional clustering within each of these domains, cross-area differences in clustering, and whether the strength of clustering was moderated by mixed selectivity.

Quantification of visual feature selectivity.

Visual responses were calculated from the median visual response latency (V3A: 46 ms; CIP: 52 ms) to the start of choice-related activity (V3A: 191 ms; CIP: 202 ms) for each population. Within these windows, individual neuron responses reflect visual selectivity without detectable choice signals (see RESULTS) (35). Except where indicated, responses were baseline subtracted. At each distance, the statistical significance of 3-D orientation tuning was tested with an ANOVA ($P < 0.05$; Bonferroni–Holm corrected for $N = 4$ distances). Significant tuning curves were fit with a Bingham function (32, 53):

$$\mathrm{R}(x) = \mathrm{DC} + \mathrm{G} \cdot \exp(-\lambda_2) \cdot \exp\left[\lambda_1 \left(\mu_1^{\mathrm{T}} x\right)^2 + \lambda_2 \left(\mu_2^{\mathrm{T}} x\right)^2\right] \quad (1)$$

Here, x is a unit vector corresponding to a given orientation, DC is an offset, G is the response gain, λ_1 sets the anisotropy of the tuning curve, and λ_2 sets the tuning bandwidth. The term $\exp(-\lambda_2)$ is a regularization parameter that ensures that G sets the gain independently of the bandwidth. The orthonormal vectors μ_1 and μ_2 are

$$\mu_1 = -\begin{bmatrix} \sin(\phi) \cdot \cos(s*) \cdot \cos(t*) + \cos(\phi) \cdot \sin(t*) \\ \sin(\phi) \cdot \cos(s*) \cdot \sin(t*) - \cos(\phi) \cdot \cos(t*) \\ -\sin(\phi) \cdot \sin(s**) \end{bmatrix}$$

$$\mu_2 = \begin{bmatrix} \sin(s*) \cdot \cos(t*) \\ \sin(s*) \cdot \sin(t*) \\ \cos(s*) \end{bmatrix} \quad (2)$$

Here, $t*$ is the preferred tilt, $s*$ is the preferred slant, and ϕ sets the axis of anisotropy by rotating the tuning curve about the preferred slant-tilt.

The preferred distance was defined as the weighted mean of the four distances, where each weight was the maximum firing rate (not baseline subtracted) across the corresponding orientation tuning curve:

$$D_{\mathrm{pref}} = \frac{\Sigma \mathrm{R}_i D_i}{\Sigma \mathrm{R}_i} \quad (3)$$

Here, D_i is the ith distance, and R_i is the maximum firing rate at that distance.

Selectivity for lower-level visual features versus higher-level 3-D object pose was quantified on a continuum by fitting the joint orientation and distance tuning curves with a separable model (24, 35, 36):

$$\mathrm{R}(\theta, D) = \mathrm{DC} + \mathrm{G} \cdot H(\theta) \cdot F(D) \quad (4)$$

Here, θ is the orientation (slant and tilt), D is the distance, DC is an offset, G is the response gain, $H(\theta)$ is the orientation tuning curve, and $F(D)$ is the distance tuning curve.

A tolerance index describing how much the shape of the orientation tuning curve depended on the distance was then calculated by taking the average of the Pearson correlations between the observed and fitted orientation tuning curves at each distance (35, 36). Values closer to 0 indicate that the shape heavily depended on distance (implying lower-level feature selectivity). Values closer to 1 indicate that the shape was more invariant to distance (implying 3-D pose tuning).

Quantification of choice- and saccade-related activity.

Choice tuning was measured from the start of choice-related activity within each area (V3A: 191 ms; CIP: 202 ms) to the end of the stimulus presentation, using frontoparallel plane trials only (35, 36). To increase statistical power, responses were pooled across distance after z scoring of all frontoparallel plane responses at each distance. Saccade tuning was measured from the start of saccade-related activity within each area (V3A: −108 ms; CIP: −102 ms) to the saccade onset. Responses were baseline subtracted.

Significant choice and saccade direction tuning curves (ANOVA, $P < 0.05$) were fit with a von Mises function:

$$\mathrm{R}(\theta) = \mathrm{DC} + \mathrm{G} \cdot \exp(-\kappa) \cdot \exp[\kappa \cdot \cos(\theta - \theta_0)] \quad (5)$$

Here, θ is the choice or saccade direction, DC is an offset, G is the response gain, κ sets the bandwidth, and θ_0 is the preference. The term $\exp(-\kappa)$ is a regularization parameter that ensures that G sets the gain independently of the bandwidth.

Discrimination indices.

To quantify how well the responses of single neurons to preferred and nonpreferred conditions could be discriminated relative to their response variability, we computed pose, choice, and saccade discrimination indexes (PDI, CDI, and SDI, respectively) (34–36, 54):

$$\mathrm{DI} = \frac{R_{\max} - R_{\min}}{R_{\max} - R_{\min} + 2 \cdot \sqrt{\frac{\mathrm{SSE}}{(N-M)}}} \quad (6)$$

Here, $R_{\max}$ and $R_{\min}$ are maximum and minimum mean responses across the tuning curve, SSE is the sum squared error around the mean response to each condition, N is the total number of trials, and M is the number of conditions (PDI: $M = 132$; CDI: $M = 8$; SDI: $M = 8$). Values closer to 0

Downloaded from journals.physiology.org/journal/jn (076.255.028.190) on April 10, 2024.

indicate weaker discriminability, whereas values closer to 1 indicate greater discriminability.

The DI reflects the difference in mean firing rates to preferred and nonpreferred conditions as well as the response variability. As such, they were correlated but distinguishable from $R_{max} - R_{min}$ [Spearman ρ; PDI: V3A = 0.66, CIP = 0.52; CDI: V3A > 0.99, CIP > 0.99 (the especially high correlations for the CDI are a consequence of the z scoring); SDI: V3A = 0.80, CIP = 0.69].

Statistical analyses.

Neuronal pairs were defined as two neurons with significant tuning simultaneously recorded on the same tetrode. For each pair, we quantified the similarity of their responses by calculating the Pearson correlation (r) between the tuning curves as well as taking absolute differences between fitted parameter values and DIs.

Differences in 3-D orientation tuning (which was measured at 4 distances) were calculated by defining vectors of each property. Each element was the parameter value from the Bingham fit at the corresponding distance. Using only distances at which both neurons in a pair had significant tuning, we took the root mean square error (RMSE) between the vectors. Absolute differences between individual parameter values and RMSEs between vectors of parameter values are both indicated with the notation $|\Delta \cdot|$.

The statistical significance of clustering was determined with permutation tests (8). For each permutation, we shuffled the spatial location of all included neurons (i.e., significantly tuned neurons from tetrodes with >1 tuned neuron) from the same area and hemisphere of the monkey. For each permuted pair, we quantified the similarity of each property. Median values were then taken across pairs. This procedure was repeated 10,000 times to generate null distributions. The P values were calculated as the proportion of null distribution values that were smaller (or larger for correlations) than the median value from the unpermuted data. Exact P values are reported unless the unpermuted median was smaller (or larger) than the minimum (or maximum) of the null distribution, in which case we report $P < 1 \times 10^{-4}$. To verify that the findings were robust to the analysis method, we also performed shuffling tests (55). The significance of the results differed in only 2 out of 32 tests. Both instances related to visual selectivity in V3A. Specifically, the clustering of tuning isotropy (λ_1) was not significant with a permutation test but was significant with a shuffling test. The clustering of tuning bandwidth (λ_2) was significant with a permutation test but not a shuffling test. Because the differences were in opposite directions, the choice in statistical test did not affect the overall conclusions. Statistics were Bonferroni–Holm corrected for multiple comparisons according to the number of comparisons within each domain: visual ($N = 8$), choice ($N = 4$), and saccade ($N = 4$).

To test for cross-area differences in the strength of clustering, we used Wilcoxon's rank-sum test to compare distributions of tuning curve correlations across pairs. We also contrasted the number of properties that clustered in each area. Importantly, we did not perform cross-area comparisons of absolute differences or RMSEs between parameter values. Such comparisons would have been problematic because the upper bound of differences in an area depends on the underlying distribution of values. For illustration, consider the extreme scenario in which all neurons prefer the same stimulus. In that case, the distribution of preference differences consists of zeros only and conclusions regarding clustering would be trivial. More generally, distributions of parameter differences will depend on other descriptive statistics (variance, skew, etc.) of the underlying distribution of values. This makes cross-area comparisons of parameter differences susceptible to inferential errors (see DISCUSSION).

To test whether the strength of clustering depended on whether the neurons showed mixed selectivity, we used a linear mixed-effects model. Specifically, the model tested whether the similarity of properties within each domain depended on whether neither, one, or both neurons in a pair were tuned in the other domains:

$$\Delta \sim b_0 + b_1 M_1 + b_2 M_2 + b_3 M_1 \cdot M_2 \quad (7)$$

Here, Δ is either the absolute difference (or RMSE) of the analyzed property or the tuning curve correlation, and M_1 and M_2 indicate selectivity in the other domains, with 0, 1, or 2 denoting the number of neurons in the pair with significant tuning. For example, the model that tested whether the similarity of saccade direction preferences ($|\Delta\theta_S|$) depended on whether the neurons had visual (V) and/or choice (C) tuning was $|\Delta\theta_S| \sim b_0 + b_1 V + b_2 C + b_3 V \cdot C$.

RESULTS

To assess the clustering of visual feature selectivity, choice-related activity, and saccade-related activity in V3A and CIP, we used correlational and parametric methods to quantify the similarity of well-isolated single neurons' spiking activity.

Clustering of Visual Feature Selectivity

Visual feature selectivity was measured by presenting 3-D oriented planar surfaces (Fig. 1*A*) at four distances (Fig. 1*B*). The monkeys simultaneously performed an eight-alternative forced-choice tilt discrimination task (Fig. 1*C*). Visually responsive neurons were identified by performing a one-way ANOVA over orientation at each distance ($P < 0.05$; Bonferroni–Holm corrected, $N = 4$). If at least one distance showed significant tuning, the neuron was classified as visually responsive (V3A: 549/692, 79%; CIP: 363/437, 83%). To assess the clustering of visual feature selectivity, we identified all tetrode recordings with at least two tuned neurons. Across those recordings, the average number of visually responsive neurons was 2.4 in both V3A (range: 2 to 4) and CIP (range: 2 to 5). In V3A, there was a total of 271 neuronal pairs from 364 neurons on 154 tetrodes (mean: 1.76 pairs/tetrode). In CIP, there were 175 pairs from 226 neurons on 95 tetrodes (mean: 1.84 pairs/tetrode).

As the first test of whether visual feature selectivity functionally clustered, we compared the 3-D pose (i.e., joint orientation and distance) tuning curves of each neuronal pair. Example tuning curves are shown for a neuronal pair from each area in Fig. 2*A*. To quantify the similarity of the tuning curves, we calculated their Pearson correlation. The distributions of correlation coefficients (r_V) are shown in Fig. 2*B* [V3A: median = 0.56, interquartile range (IQR) = 0.49; CIP: median = 0.45,

Downloaded from journals.physiology.org/journal/jn (076.255.028.190) on April 10, 2024.

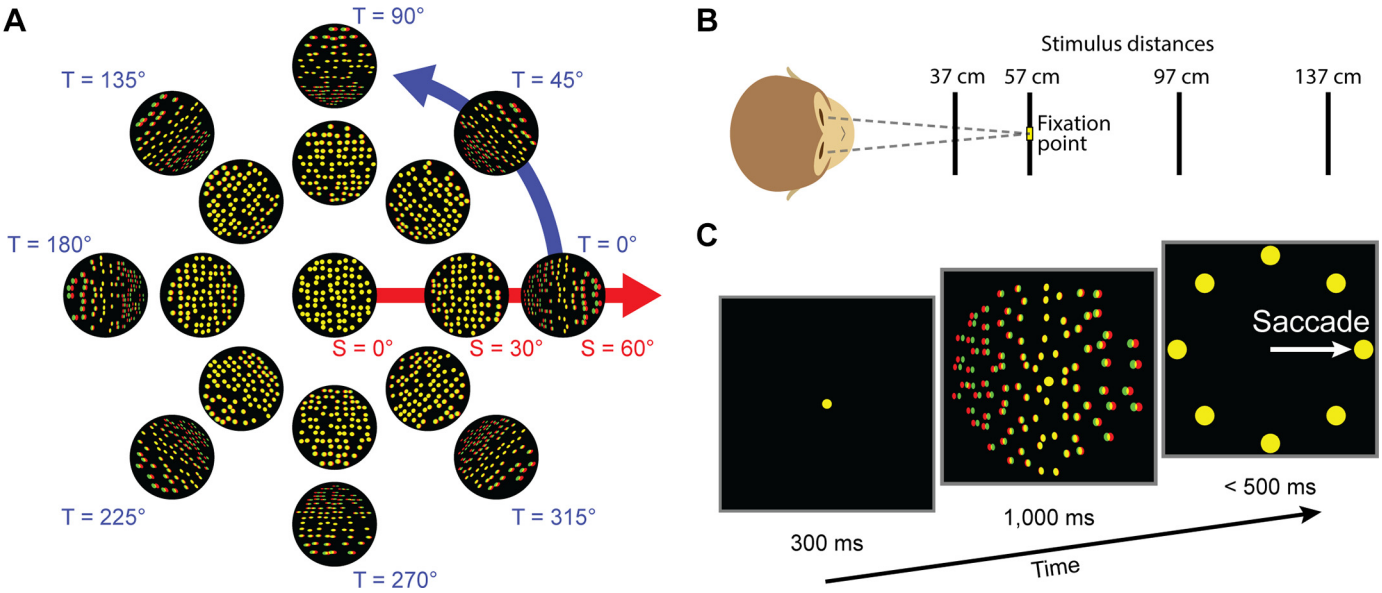


Figure 1. Visual stimuli and tilt discrimination task. *A*: slant-tilt coordinates for planar surface orientation. Tilt (T) specifies the direction that the plane is oriented in depth. Slant (S) specifies how much it is oriented in depth. Dots were rendered with perspective and stereoscopic cues (shown here as red-green anaglyphs). *B*: planes were presented at 4 distances with fixation at 57 cm. *C*: tilt discrimination task. A central target was fixated for 300 ms. A plane then appeared for 1,000 ms while fixation was maintained. The fixation target and plane then disappeared, and 8 choice targets appeared. A saccade was made to the target at the perceived nearest side of the plane.

IQR = 0.55]. In both areas, the median correlation was significantly larger than expected by chance ($P < 1 \times 10^{-4}$; Table 1, first row), indicating that visual selectivity clustered in V3A and CIP. However, the median correlation was significantly larger in V3A than CIP ($P = 1.6 \times 10^{-2}$), suggesting that the clustering was stronger in V3A.

For neurons that encode 3-D object pose, the joint tuning for orientation and distance should be multiplicatively separable (24). Consistent with 3-D pose representations being hierarchically computed, the separability of pose tuning increases between V3A and CIP (35, 36), as reflected in cross-area differences in a tolerance index that quantifies how much the 3-D orientation tuning curve shape depends on distance (MATERIALS AND METHODS, *Eq. 4*). To test whether selectivity for lower-level visual features (low tolerance values) versus higher-level 3-D object pose (high tolerance values) clustered, we took the absolute difference in tolerance values for each pair (|ΔTolerance|). The distributions of |ΔTolerance| are shown in Fig. 2*C* (V3A: median = 0.10, IQR = 0.13; CIP: median = 0.13, IQR = 0.14). Further supporting that visual selectivity was more strongly clustered in V3A, the tolerance index clustered in V3A ($P < 1 \times 10^{-4}$) but not CIP ($P = 2.4 \times 10^{-2}$; not significant after Bonferroni–Holm correction; Table 1, second row).

To test whether the strength of visual selectivity clustered, we calculated a pose discrimination index for each neuron (PDI; MATERIALS AND METHODS, *Eq. 6*). For each pair, we then took the absolute difference between the PDI values (|ΔPDI|). The distributions of |ΔPDI| are shown in Fig. 2*D* (V3A: median = 0.05, IQR = 0.07; CIP: median = 0.05, IQR = 0.07; same values due to rounding). Although the median differences in PDI values were nearly identical, the strength of selectivity significantly clustered in V3A ($P = 3 \times 10^{-4}$) but not CIP ($P = 4.7 \times 10^{-2}$; not significant after Bonferroni–Holm correction; Table 1, third row). This again supports stronger clustering of visual selectivity in V3A and highlights that clustering measures based on differences in selectivity must be interpreted relative to the underlying distribution of values within the area (see MATERIALS AND METHODS and DISCUSSION).

We next examined the clustering of orientation selectivity by performing parametric comparisons of Bingham function fits to the orientation tuning curves (MATERIALS AND METHODS, *Eqs. 1* and *2*) (32, 34–36). An example orientation tuning curve measured at 57 cm along with its Bingham function fit is shown for a V3A neuron in Fig. 3*A*. Using the fitted parameter values, we compared four properties: orientation preference (θ), tuning bandwidth (λ_2), tuning anisotropy (λ_1), and the axis of anisotropy about the preferred slant-tilt (ϕ). Schematics illustrating how orientation tuning depends on these parameters are shown in Fig. 4.

To quantify the clustering of orientation preference, we computed for each pair the RMSE between preferred orientations at distances that both neurons were tuned ($|\Delta\theta_V|$) (MATERIALS AND METHODS). As such, only pairs with at least one distance at which both neurons were tuned were included (V3A: 253/271 pairs; CIP: 166/175 pairs). The distributions of $|\Delta\theta_V|$ are shown in Fig. 3*B* (V3A: median = 40°, IQR = 37°; CIP: median = 48°, IQR = 36°). In both areas, the median $|\Delta\theta_V|$ was significantly smaller than expected by chance ($P < 1 \times 10^{-4}$; Table 1, fourth row), indicating that orientation preference clustered in V3A and CIP.

We next tested whether tuning bandwidth clustered by computing for each pair the RMSE between λ_2 values at distances that both neurons were tuned ($|\Delta\lambda_2|$). The distributions of $|\Delta\lambda_2|$ are shown in Fig. 3*C* (V3A: median = 0.73, IQR = 1.06; CIP: median = 0.79, IQR = 1.20). Further supporting that visual selectivity was more strongly clustered in V3A, tuning bandwidth significantly clustered in V3A ($P = 8.9 \times 10^{-3}$) but not CIP ($P = 0.17$; Table 1, fifth row).

Downloaded from journals.physiology.org/journal/jn (076.255.028.190) on April 10, 2024.

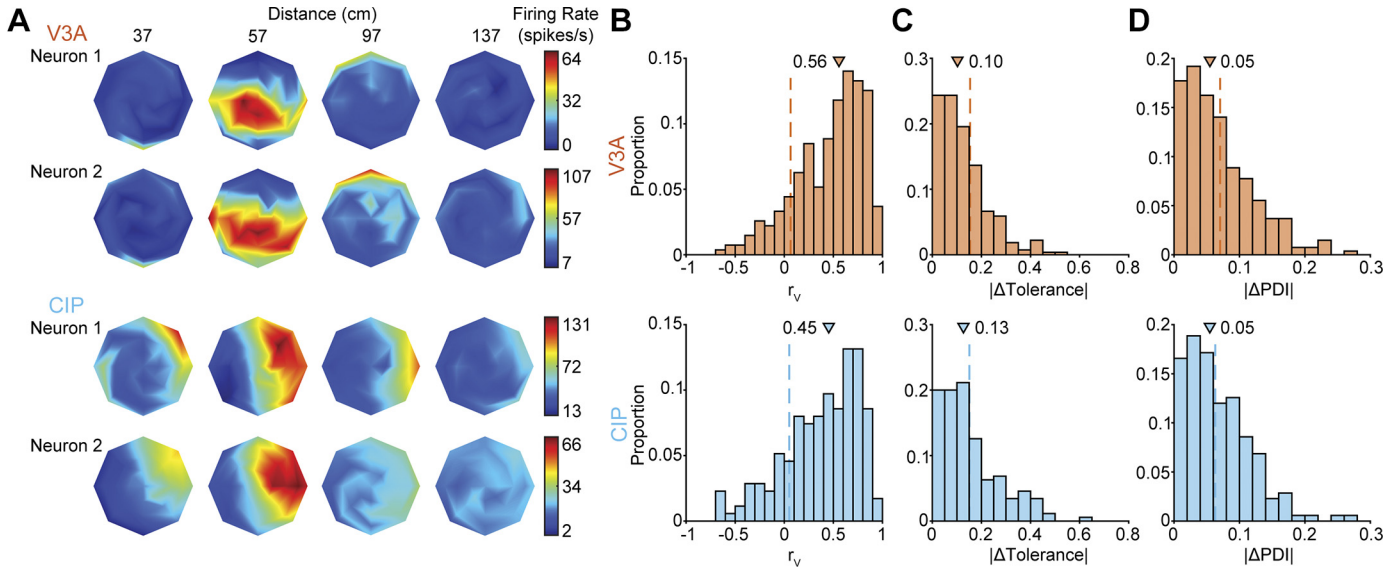


Figure 2. Clustering of 3-dimensional (3-D) pose tuning. *A*: example tuning curves of neuronal pairs from V3A [Pearson correlation (r_V) = 0.91 and absolute differences in tolerance of 3-D orientation tuning curve shape to distance (|ΔTolerance|) = 0.12, pose discrimination index (|ΔPDI|) = 0.02, orientation preference ($|\Delta\theta_V|$) = 15°, tuning bandwidth ($|\Delta\lambda_2|$) = 1.21, tuning anisotropy ($|\Delta\lambda_1|$) = 3.20, axis of tuning anisotropy ($|\Delta\phi|$) = 30°, and distance preferences (|Δ*D*|) = 4 cm] and caudal intraparietal area (CIP) (r_V = 0.80, |ΔTolerance| = 0.03, |ΔPDI| = 0.05, $|\Delta\theta_V|$ = 17°, $|\Delta\lambda_2|$ = 0.78, $|\Delta\lambda_1|$ = 0.59, $|\Delta\phi|$ = 18°, |Δ*D*| = 13 cm). Heat maps show 3-D orientation tuning at each distance, plotted in slant-tilt coordinates (Fig. 1*A*). *B*: r_V between tuning curves of neuronal pairs in V3A (*top*, orange) and CIP (*bottom*, blue). *C*: |ΔTolerance|. *D*: |ΔPDI|. In *B*–*D*, triangles mark median values. Dashed vertical lines mark median values obtained by chance.

Finally, we tested whether the amount of anisotropy in the orientation tuning curve (λ_1) and axis about which anisotropies occurred (ϕ) clustered by calculating corresponding RMSEs ($|\Delta\lambda_1|$ and $|\Delta\phi|$, respectively). The distributions of $|\Delta\lambda_1|$ are shown in Fig. 3*D* (V3A: median = 3.63, IQR = 6.47; CIP: median = 2.95, IQR = 5.08). Tuning anisotropy was not clustered in either area ($P \geq 0.28$; Table 1, sixth row). The distributions of $|\Delta\phi|$ are shown in Fig. 3*E* (V3A: median = 31°, IQR = 32°; CIP: median = 35°, IQR = 27°). In this case, there was clustering in V3A ($P < 1 \times 10^{-4}$) but not CIP ($P = 0.38$; Table 1, seventh row), indicating that whereas the amount of anisotropy did not cluster in either area, the axis about which anisotropies occurred did cluster in V3A.

As the final test of whether visual feature selectivity clustered, we compared the distance preferences of each pair. The preferred distance (D_{pref}) of each neuron was estimated by calculating the weighted average of stimulus distances with each distance weighted by the maximum firing rate across the corresponding orientation tuning curve (MATERIALS AND METHODS, *Eq. 3*). For each pair, we then took the absolute difference between the preferred distances (|Δ*D*|). The distributions of |Δ*D*| are shown in Fig. 5 (V3A: median = 10 cm, IQR = 22 cm; CIP: median = 13 cm, IQR = 22 cm). The median |Δ*D*| was significantly smaller than expected by chance in V3A ($P = 1 \times 10^{-4}$) but not CIP ($P = 5.3 \times 10^{-2}$; Table 1, eighth row), further supporting that visual feature selectivity was more strongly clustered in V3A.

The above analyses indicate that visual feature selectivity clustered in both areas. However, the tuning curves of neuronal pairs were more strongly correlated in V3A. In addition, substantially more properties clustered in V3A (7/8 comparisons) than in CIP (2/8 comparisons, with clustering attributable to the local similarity of orientation preferences only). These findings collectively imply that visual selectivity was more strongly clustered in V3A than in CIP.

Table 1. *Clustering of visual feature selectivity*

Response Property	*P* Value	
	V3A	CIP
Tuning correlation (r_V)	**$<1 \times 10^{-4}$**	**$<1 \times 10^{-4}$**
Tolerance index	**$<1 \times 10^{-4}$**	2.4×10^{-2}
Pose discrimination index (PDI)	**3×10^{-4}**	4.7×10^{-2}
Orientation preference (θ_V)	**$<1 \times 10^{-4}$**	**$<1 \times 10^{-4}$**
Tuning bandwidth (λ_2)	**8.9×10^{-3}**	0.17
Tuning anisotropy (λ_1)	0.33	0.28
Axis of anisotropy (ϕ)	**$<1 \times 10^{-4}$**	0.38
Distance preference (*D*)	**1×10^{-4}**	5.3×10^{-2}

Significant *P* values indicating clustering are in bold (Bonferroni–Holm corrected, *N* = 8 comparisons). CIP, caudal intraparietal area.

Clustering of Choice-Related Activity

We next identified neurons that carried choice-related activity during the tilt discrimination task by testing whether their responses to frontoparallel planes (which were task ambiguous) covaried with the monkey's choices (ANOVA, $P < 0.05$; Fig. 6*A*). Across the populations, 25% (172/692) of the V3A and 46% (201/437) of the CIP neurons had significant choice tuning that began in V3A 191 ms after stimulus onset and in CIP 202 ms after (35, 36). As a control, we confirmed that before these time points the prevalence of choice activity was consistent with the expected rate of false positives (V3A: 7%, 46/692; CIP: 5%, 22/437). That activity was also not associated with whether the neurons were classified as

Downloaded from journals.physiology.org/journal/jn (076.255.028.190) on April 10, 2024.

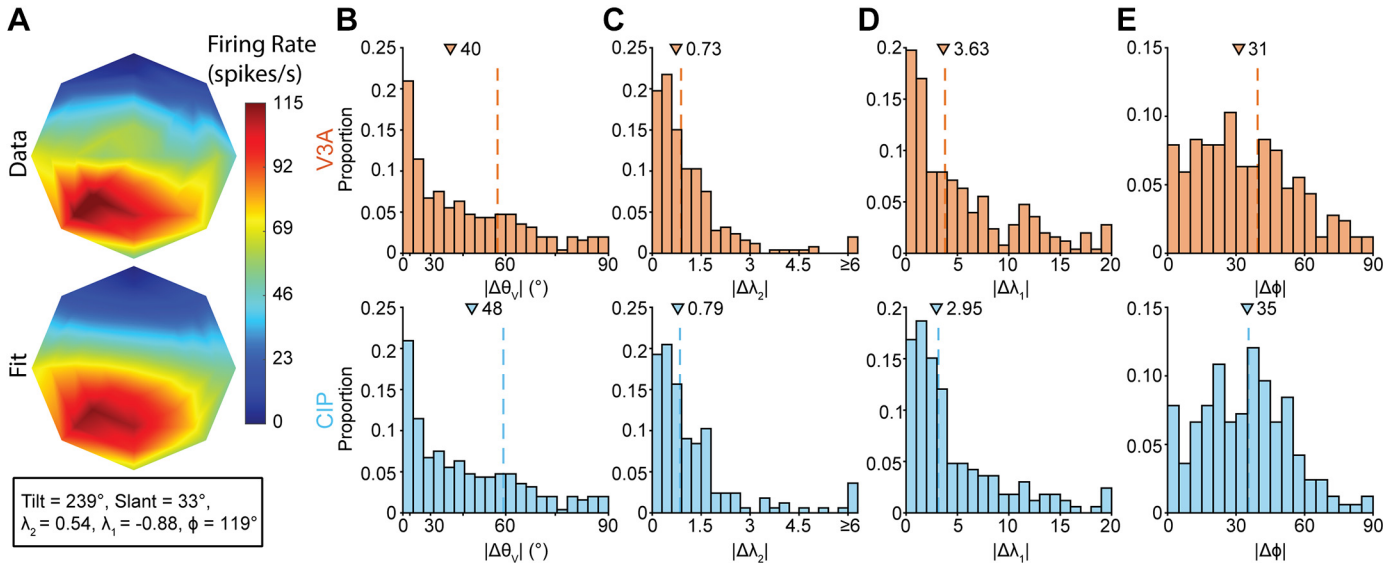


Figure 3. Clustering of 3-dimensional (3-D) orientation tuning. *A*: example tuning curve from V3A (*top*) with Bingham fit ($r = 0.96$; *bottom*). *Inset*, the Bingham parameter values. *B*: absolute differences in the orientation preferences of neuronal pairs ($|\Delta\theta_V|$) in V3A (*top*, orange) and caudal intraparietal area (CIP) (*bottom*, blue), plotted over an equal area axis. *C*: absolute differences in tuning bandwidths ($|\Delta\lambda_2|$). *D*: absolute differences in tuning anisotropies ($|\Delta\lambda_1|$). *E*: absolute differences in the axes of tuning anisotropy ($|\Delta\phi|$). In *B*–*E*, triangles mark median values. Dashed vertical lines mark median values obtained by chance.

carrying choice-related activity, since only 16 of the 46 V3A and 13 of the 22 CIP neurons had choice tuning during the choice analysis window (35). To assess the clustering of choice-related activity, we identified all tetrode recordings with at least two tuned neurons. Across those recordings, the average number of neurons with choice-related activity was 2.2 (range: 2 to 4) in both areas. In V3A, there was a total of 44 pairs from 68 neurons on 31 tetrodes (mean: 1.42 pairs/tetrode). In CIP, there were 66 pairs from 103 neurons on 47 tetrodes (mean: 1.40 pairs/tetrode).

Example choice tuning curves are shown for a neuronal pair from each area in Fig. 6*B*. To quantify the similarity of the tuning curves, we calculated their Pearson correlation. The distributions of correlation coefficients (r_C) are shown in

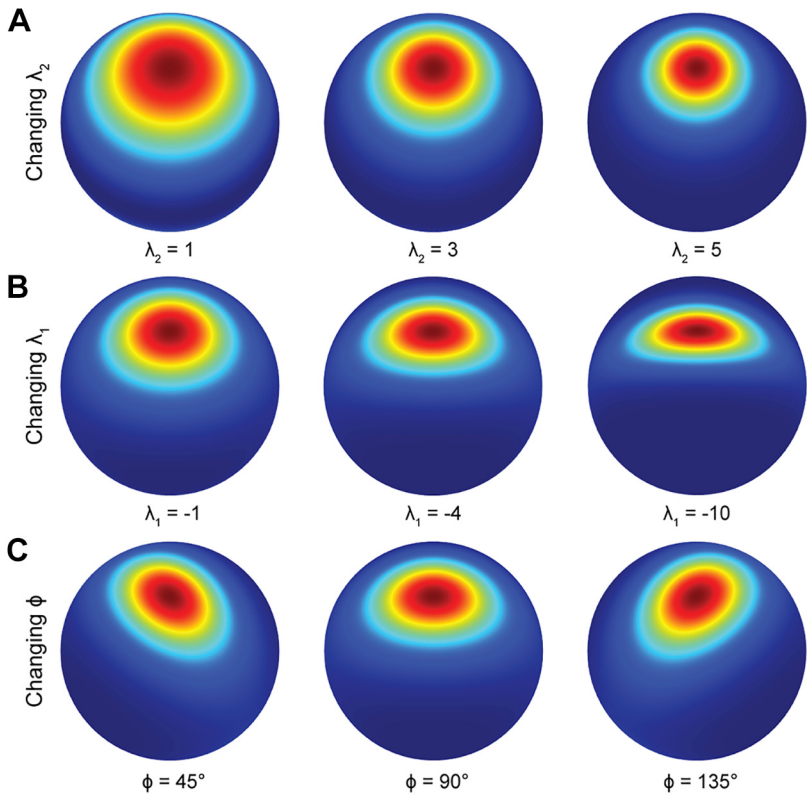


Figure 4. Bingham parameters. To illustrate how orientation tuning depends on parameters λ_2 (tuning bandwidth), λ_1 (tuning anisotropy), and ϕ (axis of tuning anisotropy), tuning curves were modeled with a preferred tilt of 90° and slant of 30°. *A*: changing λ_2 with $\lambda_1 = 0$. *B*: changing λ_1 with $\lambda_2 = 3$ and $\phi = 90°$. *C*: changing ϕ with $\lambda_1 = -2.5$ and $\lambda_2 = 3$.

Downloaded from journals.physiology.org/journal/jn (076.255.028.190) on April 10, 2024.

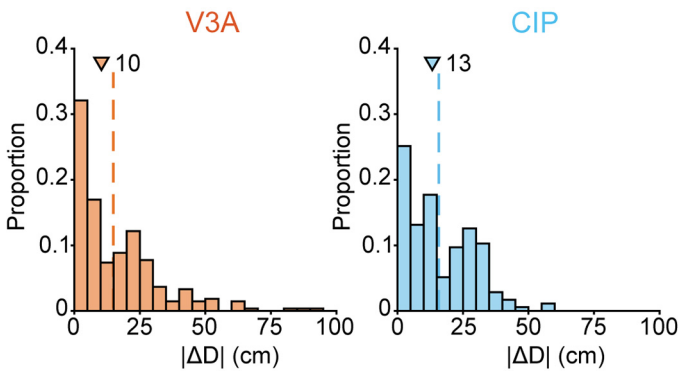


Figure 5. Clustering of preferred distance. Absolute differences in the distance preferences of neuronal pairs (|Δ*D*|) in V3A (*left*, orange) and caudal intraparietal area (CIP) (*right*, blue). Triangles mark median values. Dashed vertical lines mark median values obtained by chance.

Fig. 6*C* (V3A: median = 0.73, IQR = 0.57; CIP: median = 0.72, IQR = 0.57). In both areas, the median correlation was significantly larger than expected by chance ($P \leq 3 \times 10^{-4}$; Table 2, first row), indicating that choice-related activity clustered in V3A and CIP. The median correlations were not significantly different across the areas ($P = 0.57$). Thus, choice-related activity was substantially more prevalent in CIP than V3A, but the local similarity of choice tuning (when present) was similar in the two areas.

To determine which features of the choice-related activity clustered, we fit each tuning curve with a von Mises function (MATERIALS AND METHODS, *Eq. 5*; Fig. 6*B*, solid curves). We then quantified the clustering of choice preferences (θ_C) by taking the absolute difference between the preferences of each pair ($|\Delta\theta_C|$). The distributions of $|\Delta\theta_C|$ are shown in Fig. 6*D* (V3A: median = 13°, IQR = 77°; CIP: median = 22°, IQR = 65°). The median $|\Delta\theta_C|$ was significantly smaller than expected by chance in both areas ($P < 1 \times 10^{-4}$; Table 2, second row), indicating that choice preferences clustered in V3A and CIP. We likewise assessed the clustering of tuning bandwidths (half-width at half-height; $HWHH_C$) by taking their absolute difference for each pair ($|\Delta HWHH_C|$). The distributions of $|\Delta HWHH_C|$ are shown in Fig. 6*E* (V3A: median = 16°, IQR = 16°; CIP: median = 14°, IQR = 23°). Choice tuning bandwidth was not significantly clustered in V3A ($P = 0.25$) but was clustered in CIP ($P = 2.7 \times 10^{-3}$; Table 2, third row), suggesting that choice-related activity was more strongly clustered in CIP.

Finally, we tested whether the strength of choice selectivity clustered by calculating a choice discrimination index for each neuron (CDI; MATERIALS AND METHODS, *Eq. 6*). For each pair, we then took the absolute difference between the CDI values (|ΔCDI|). The distributions of |ΔCDI| are shown in Fig. 6*F* (V3A: median = 0.06, IQR = 0.06; CIP: median = 0.05, IQR = 0.07). The strength of choice selectivity was not significantly clustered in V3A ($P = 0.37$) but was clustered in CIP ($P = 4.5 \times 10^{-2}$; Table 2, fourth row), supporting that clustering was stronger in CIP.

The above analyses indicate that choice-related activity clustered in both areas. However, more properties clustered in CIP (4/4 comparisons) than in V3A (2/4 comparisons, with clustering attributable to the local similarity of choice preferences only). Although visual and choice preferences tend to align in both areas (35, 36), the present findings reveal stronger clustering of visual selectivity in V3A and stronger clustering of choice activity in CIP. This may reflect differences in the areas' computational roles, with V3A having a greater role in visual signal processing and CIP having a greater role in 3-D perceptual decision processes.

Clustering of Saccade-Related Activity

We further identified neurons that carried saccade-related activity during a visually guided saccade task by testing whether the activity depended on the saccade direction (ANOVA, $P < 0.05$; Fig. 7*A*). Across the populations, 60% (415/692) of V3A and 63% (274/437) of CIP neurons carried saccade-related activity that predicted the direction and timing of eye movements (35, 36). That activity began in V3A 108 ms before the saccade and in CIP 102 ms before. Importantly, the saccade-related activity was functionally distinct from the choice-related activity (35, 36). To assess the clustering of saccade-related activity, we identified all tetrode recordings with at least two tuned neurons. Across those recordings, the average number of neurons with saccade-related activity was 2.3 (range: 2 to 4) in both areas. In V3A, there were 160 pairs from 224 neurons on 97 tetrodes (mean: 1.65 pairs/tetrode). In CIP, there were 99 pairs from 152 neurons on 67 tetrodes (mean: 1.48 pairs/tetrode).

Example saccade direction tuning curves are shown for a neuronal pair from each area in Fig. 7*B*. To quantify the similarity of the tuning curves, we calculated their Pearson correlation. The distributions of correlation coefficients (r_S) are shown in Fig. 7*C* (V3A: median = 0.77, IQR = 0.38; CIP: median = 0.66, IQR = 0.72). In both areas, the median correlation was significantly larger than expected by chance ($P < 1 \times 10^{-4}$; Table 3, first row), indicating that saccade-related activity clustered in V3A and CIP. However, the median correlation was significantly larger in V3A than CIP ($P = 1.8 \times 10^{-3}$), suggesting that the clustering was stronger in V3A.

To determine which features of the saccade-related activity clustered, we fit each saccade direction tuning curve with a von Mises function (MATERIALS AND METHODS, *Eq. 5*; Fig. 7*B*, solid curves). We then quantified the clustering of saccade direction preferences (θ_S) by taking the absolute difference between the preferences of each pair ($|\Delta\theta_S|$). The distributions of $|\Delta\theta_S|$ are shown in Fig. 7*D* (V3A: median = 17°, IQR = 30°; CIP: median = 28°, IQR = 60°). The median $|\Delta\theta_S|$ was significantly smaller than expected by chance in both areas ($P < 1 \times 10^{-4}$; Table 3, second row), indicating that the direction preferences clustered in V3A and CIP. We likewise assessed the clustering of tuning bandwidths ($HWHH_S$) by taking their absolute difference for each pair ($|\Delta HWHH_S|$). The distributions of $|\Delta HWHH_S|$ are shown in Fig. 7*E* (V3A: median = 10°, IQR = 17°; CIP: median = 14°, IQR = 18°). Saccade direction tuning bandwidth was significantly clustered in V3A ($P = 7 \times 10^{-4}$) but not CIP ($P = 3.3 \times 10^{-2}$, not significant after Bonferroni–Holm correction; Table 3, third row), supporting that clustering was stronger in V3A.

Finally, we tested whether the strength of saccade direction selectivity clustered by calculating a saccade discrimination index for each neuron (SDI; MATERIALS AND METHODS,

Downloaded from journals.physiology.org/journal/jn (076.255.028.190) on April 10, 2024.

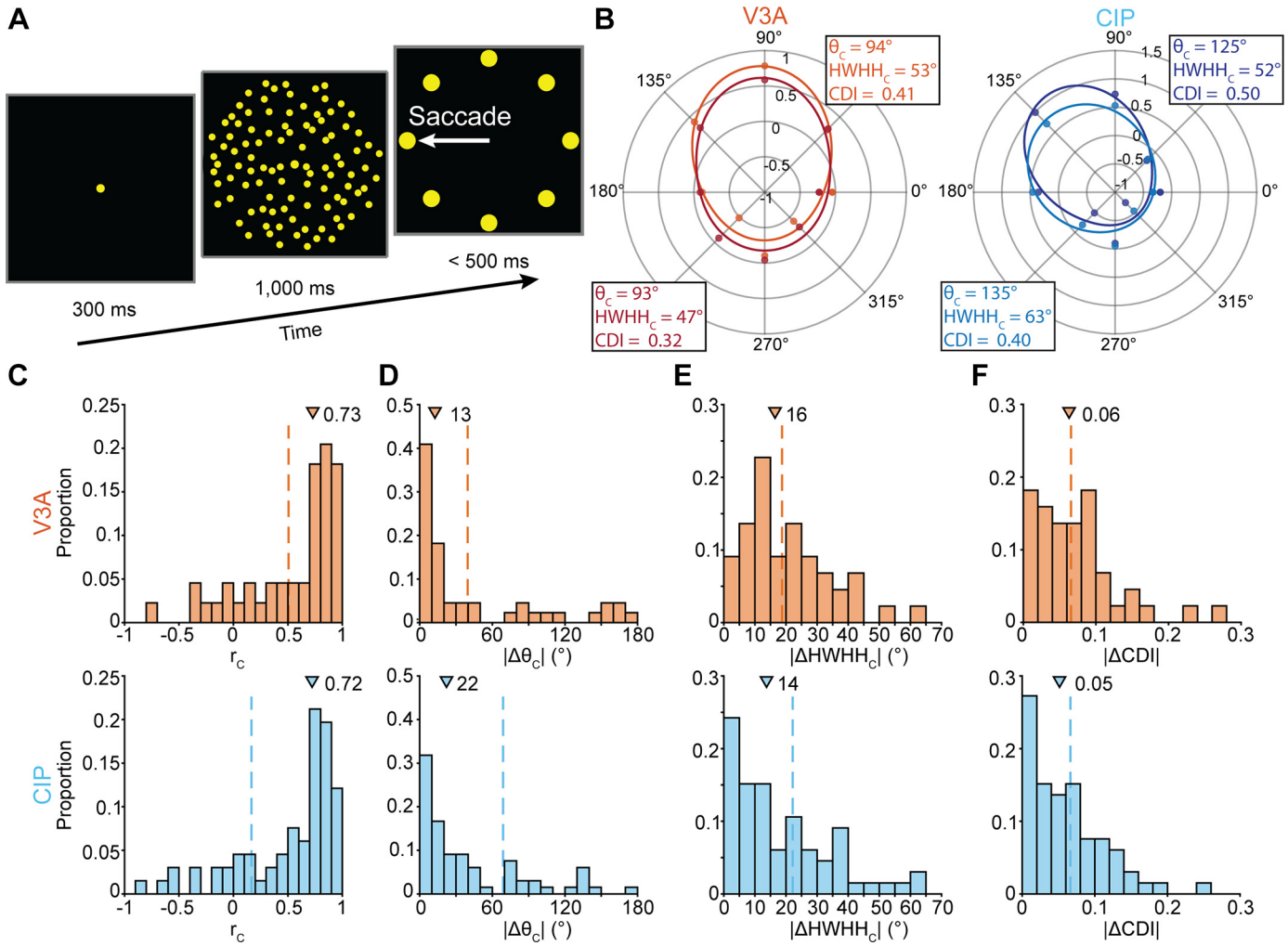


Figure 6. Clustering of choice-related activity. *A*: choice activity was measured during the presentation of frontoparallel planes, which were task ambiguous (cf. Fig. 1*C*). *B*: example tuning curves of neuronal pairs from V3A [*left*; Pearson correlation (r_C) = 0.91 and absolute differences in choice preference ($|\Delta\theta_C|$) = 1°, half-width at half-height ($|\Delta HWHH_C|$) = 6°, and choice discrimination index |ΔCDI| = 0.09] and caudal intraparietal area (CIP) (*right*; r_C = 0.97, $|\Delta\theta_C|$ = 10°, $|\Delta HWHH_C|$ = 11°, |ΔCDI| = 0.10). Colors correspond to different neurons. Data points are mean *z*-scored responses, and curves are von Mises fits. *Insets*, θ_C, $HWHH_C$, and CDI. *C*: r_C between tuning curves of neuronal pairs in V3A (*top*, orange) and CIP (*bottom*, blue). *D*: $|\Delta\theta_C|$. *E*: $|\Delta HWHH_C|$. *F*: |ΔCDI|. In *C*–*F*, triangles mark median values. Dashed vertical lines mark median values obtained by chance.

Eq. 6). For each pair, we then took the absolute difference between the SDI values (|ΔSDI|). The distributions of |ΔSDI| are shown in Fig. 7*F* (V3A: median = 0.07, IQR = 0.10; CIP: median = 0.09, IQR = 0.10). The strength of saccade direction selectivity was significantly clustered in V3A ($P < 1 \times 10^{-4}$) but not CIP ($P = 0.40$; Table 3, fourth row), further supporting that clustering was stronger in V3A.

Table 2. *Clustering of choice-related activity*

Response Property	*P* Value	
	V3A	CIP
Tuning correlation (r_C)	**3×10^{-4}**	**$<1 \times 10^{-4}$**
Choice preference (θ_C)	**$<1 \times 10^{-4}$**	**$<1 \times 10^{-4}$**
Tuning bandwidth ($HWHH_C$)	0.25	**2.7×10^{-3}**
Choice discrimination index (CDI)	0.37	**4.5×10^{-2}**

Significant *P* values indicating clustering are in bold (Bonferroni–Holm corrected, $N = 4$ comparisons). CIP, caudal intraparietal area.

The above analyses indicate that saccade-related activity clustered in both areas. However, the tuning curves of neuronal pairs were more strongly correlated in V3A. In addition, more properties clustered in V3A (4/4 comparisons) than in CIP (2/4 comparisons, with clustering attributable to the local similarity of saccade direction preferences only). Stronger clustering of visual selectivity and saccade-related activity in V3A than in CIP may reflect a greater role for V3A in the parallel processing of visual and oculomotor-related signals. In contrast, stronger clustering of choice-related activity in CIP than in V3A may reflect a greater role for CIP in 3-D perceptual decision processes and the synthesis of visual and oculomotor signals (35, 36).

Clustering Had Little to No Dependence on Mixed Selectivity

Having assessed the clustering of visual and choice- and saccade-related activity, we finally tested whether the strength of clustering depended on whether the neurons

Downloaded from journals.physiology.org/journal/jn (076.255.028.190) on April 10, 2024.

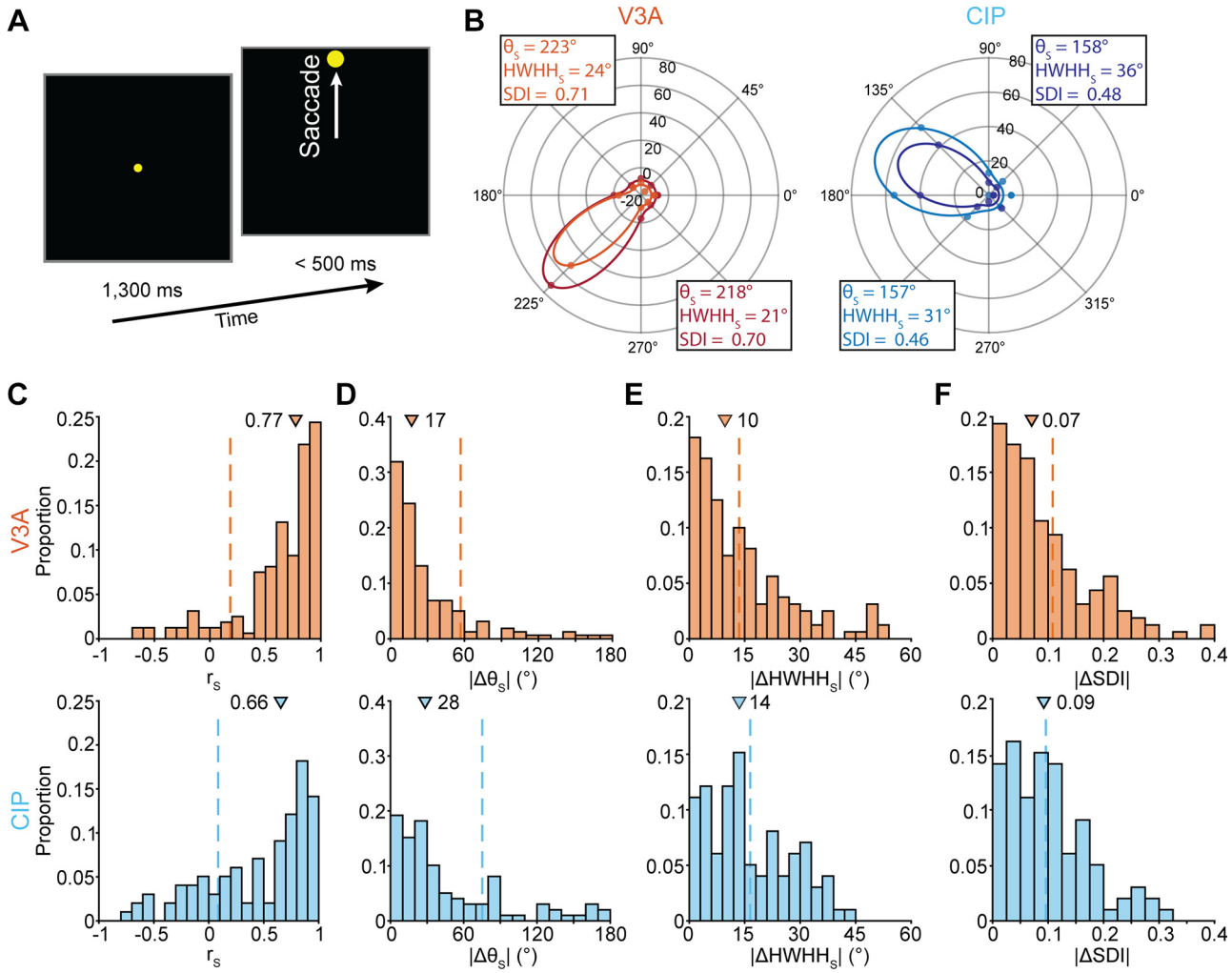


Figure 7. Clustering of saccade-related activity. *A*: visually guided saccade task. A central target was fixated for 1,300 ms. The fixation target then disappeared, and a saccade target appeared at 1 of 8 locations. A saccade was then made to that target. *B*: example tuning curves of neuronal pairs from V3A [*left*; Pearson correlation (r_S) = 0.99 and absolute differences in saccade direction preferences ($|\Delta\theta_S|$) = 5°, half-width at half-height ($|\Delta HWHH_S|$) = 3°, and saccade discrimination index ($|\Delta SDI|$) = 0.01] and caudal intraparietal area (CIP) (*right*; r_S = 0.97, $|\Delta\theta_S|$= 1°, $|\Delta HWHH_S|$ = 5°, $|\Delta SDI|$ = 0.02). Colors correspond to different neurons. Data points are mean responses, and curves are von Mises fits. *Insets*, θ_S, $HWHH_S$, and SDI. *C*: r_S between tuning curves of neuronal pairs in V3A (*top*, orange) and CIP (*bottom*, blue). *D*: $|\Delta\theta_S|$. *E*: $|\Delta HWHH_S|$. *F*: $|\Delta SDI|$. In *C*–*F*, triangles mark median values. Dashed vertical lines mark median values obtained by chance.

showed mixed selectivity. We first compared the prevalence of unimodal and mixed selectivity across the two areas. As indicated above, nearly twice as many CIP (46%) as V3A (25%) neurons carried choice-related activity (35, 36). To further compare the prevalence of mixed visual and saccade signals, we marginalized over the presence/absence of choice activity. Across the V3A neurons recorded on tetrodes with more than one neuron (N = 493), 58 (12%) showed neither visual selectivity nor saccade activity, 151 (31%) showed visual selectivity only, 40 (8%) showed saccade activity only, and 244 (49%) showed both visual and saccade activity. A similar pattern was observed across the corresponding 292 CIP neurons: 24 (8%) showed neither visual selectivity nor saccade activity, 85 (29%) showed visual selectivity only, 25 (9%) showed saccade activity only, and 158 (54%) showed both visual and saccade activity. Thus, the prevalence of visual selectivity only, saccade-related activity only, and mixed selectivity was similar in the two areas.

Table 3. *Clustering of saccade-related activity*

Response Property	*P* Value	
	V3A	CIP
Tuning correlation (r_S)	**$<1\times10^{-4}$**	**$<1\times10^{-4}$**
Saccade direction preference (θ_S)	**$<1\times10^{-4}$**	**$<1\times10^{-4}$**
Tuning bandwidth ($HWHH_S$)	**7×10^{-4}**	3.3×10^{-2}
Saccade discrimination index (SDI)	**$<1\times10^{-4}$**	0.40

Significant P values indicating clustering are in bold (Bonferroni-Holm corrected, N = 4 comparisons). CIP, caudal intraparietal area.

We finally tested whether the strength of clustering within each domain depended on whether the neurons showed selectivity in the other domains. For each examined property (32 total: 8 visual, 4 choice, and 4 saccadic from 2 areas), we used a linear mixed-effects model to test whether the similarity between neuronal pairs depended on whether neither,

Downloaded from journals.physiology.org/journal/jn (076.255.028.190) on April 10, 2024.

one, or both neurons were tuned in the other domains (*Eq. 7*). For 31/32 comparisons, there was no significant relationship ($P \geq 0.11$). The only significant case was that saccade direction preferences in CIP tended to be more similar if both neurons showed choice tuning ($b_1 = -24.9$, $P = 4.5 \times 10^{-3}$). These results indicate that mixed selectivity had little to no bearing on within-domain functional clustering.

DISCUSSION

In this study, we assessed whether the visual feature selectivity, choice-related activity, and saccade-related activity of neurons in macaque areas V3A and CIP functionally cluster. In both areas, we found statistically significant clustering of tuning preferences in all three domains. However, there were also domain-specific, cross-area differences in the clustering of other properties such as bandwidth, and therefore the overall strength of clustering. Area V3A showed stronger clustering of visual selectivity and saccade-related activity. Area CIP showed stronger clustering of choice-related activity. The clustering of neurons with similar functional properties is thought to facilitate computations within the clustered feature space (1–7, 22). As such, cross-area differences in clustering may provide insights into the functional roles of the areas. Stronger clustering of visual and saccade signals in V3A may reflect wiring patterns that are optimized for within-domain (visual or oculomotor, though often multiplexed) processing that supports the subsequent computation of invariant object representations and sensorimotor transformations. Consistent with this possibility, V3A neurons that carry saccade-related activity are less selective for high-level 3-D visual features than those without saccade-related activity (36). Stronger clustering of choice-related activity in CIP may likewise reflect wiring that is optimized to synthesize those visual and oculomotor signals. Given the relative sparsity of V3A pairs for which both neurons carried choice activity, some caution is required in concluding cross-area differences based on that finding alone. However, the interpretation is bolstered by the substantially greater prevalence of choice signals in CIP and the finding that choice signals moderated the strength of sensorimotor associations (which were stronger in CIP) (34–36). Finally, we found that the strength of within-domain clustering did not depend on whether the neurons showed mixed selectivity.

Considering that V3A receives direct input from V1 and V2 (25, 26) and is traditionally classified as a visual area, it may be surprising that it showed stronger clustering of saccade-related activity than CIP. It is therefore important to emphasize that extraretinal signals modulate visual responses in V3A, that saccade-related activity in V3A predicts the direction and timing of saccades, and that V3A shows sensorimotor associations between visual and saccade direction preferences (albeit weaker than in CIP) (36–41). The present data are consistent with a predominantly bottom-up saccade signal given that the activity began 6 ms earlier in V3A than in CIP and that the time course of CIP activity closely matched the temporally integrated V3A activity (36). However, other work suggests that corollary discharge supports saccadic remapping in V3A (41). These findings collectively suggest that V3A and CIP contain bottom-up and top-down saccade signals. Clarifying the origins of oculomotor signals in these areas and how they support visuomotor behavior will require further studies to characterize pre- and postsaccadic activity and whether that activity depends on the task or training history. Our findings further implicate V3A in oculomotor processing, support the reclassification of V3A as association cortex, and suggest that classical notions of sensorimotor dichotomies break down faster as information ascends the dorsal visual pathway than is generally thought.

The PPC of multiple species is widely implicated in transforming sensory information into decisions and motor responses (11, 56–60). In contrast to a linear cascade from sensory to motor representations across the cortical hierarchy, the present findings suggest that parallel processing of sensory and motor-related signals can occur within the same lower-level area, after which downstream, higher-level targets synthesize that information to bridge perception and action. In particular, the prevalence of mixed visual and saccade signals in V3A and CIP did not substantially differ, but the greater prevalence of choice signals in CIP was associated with stronger sensorimotor associations (35, 36). Among other PPC areas and functions, it is conceivable that similar architectures support evidence accumulation, categorical learning, and motor planning in the lateral intraparietal area (13, 61–63), the coordination of hand movements based on visual and proprioceptive signals in the medial intraparietal area (64, 65), as well as spatial and self-motion processing in the ventral intraparietal area (18, 66, 67). Testing this possibility will require the prevalence of mixed selectivity across hierarchical areas to be contrasted with the strength of sensory-sensory and/or sensory-motor associations.

Previous studies reported functional correlations between V3A/CIP activity and behavioral choices during 3-D discrimination tasks (31, 34–36). However, there is little evidence for causal relationships between these areas and 3-D perception. To our knowledge, no study has tested the perceptual effects of causally manipulating V3A. Two studies tested the perceptual effects of reversibly inactivating CIP with muscimol, but the results were limited. In the first study, the injections impaired performance in a delayed match-to-sample task for surface tilt but in only half of the experiments (68). In the second study, the injections resulted in a relatively small deficit in 3-D curvature discrimination (45). Because the perceptual effects of causal manipulations depend on clustering (69), the present findings provide essential information for studies assessing the causal roles of these areas in sensory and motor processing. In particular, the findings support the feasibility of such experiments, so long as the cross-area differences in clustering of visual selectivity, choice-related activity, and saccade-related activity are considered. For example, the differences may translate into larger 3-D perceptual effects when V3A is causally manipulated despite the fact that CIP is functionally more strongly associated with 3-D visual processing (27, 34–36). This may also relate to the limited behavioral effects of CIP inactivation in previous studies.

Some of our analyses showed that the similarity of a given property was comparable in the two areas, but clustering was statistically significant in only one. For instance, the summary statistics for the pose discrimination index in V3A and CIP were nearly identical, but clustering was only significant in V3A. Such cases highlight that clustering measures based on differences in property values must be interpreted

Downloaded from journals.physiology.org/journal/jn (076.255.028.190) on April 10, 2024.

relative to the underlying distribution of values. For example, random sampling of pairs from a narrower underlying distribution will produce smaller average pairwise differences than if the underlying distribution was broader. As such, the magnitude of pairwise differences alone is not sufficient to draw conclusions about clustering. Moreover, the dependence of such measures on the underlying distributions implies that they generally cannot be used to perform direct comparisons of clustering across areas. Instead, it is necessary to determine whether the observed differences are smaller than expected by chance given the underlying distribution (e.g., using resampling methods). For this reason, our cross-area comparisons were based on the correlations between the tuning curves of neuronal pairs and the proportion of properties with significant clustering.

The use of tetrode recordings facilitated the assessment of functional clustering based on direct comparisons of single-neuron responses. Although our focus was on the local similarity of tuning properties, our findings are consistent with the possibility of topographic maps of visual, choice, and saccade preferences. However, it was not possible to test for such maps because the penetration trajectories were always dorsal-ventral, resulting in approach vectors that were often not ideal for estimating layer/columnar information. The columnar organization of V3A and CIP can nevertheless be investigated with laminar probes like those used here by carefully selecting trajectories according to the convolutions of the cortical sheet. As such, the mesoscopic organization of visual, choice, and saccade properties in V3A and CIP as well as any relationships between feature maps remain topics for future studies.

DATA AVAILABILITY

The data analyzed in this article are available through the Open Science Framework via our laboratory's profile at https://osf.io/8wxk7/.

ACKNOWLEDGMENTS

We thank Lowell W. Thompson for helpful discussions about the analyses.

GRANTS

This work was supported by NIH Grants EY029438 and EY035005. Z.Z. was partially supported by a Walsh Graduate Student Support Initiative award from the McPherson Eye Research Institute. B.K. was partially supported by NIH Grant NS128586. R.D. was partially supported by NIH Grant EY027721 and National Science Foundation (NSF) Grant DGE-1545481. A.R. was partially supported by NIH Grant NS105602. Further support was provided by NIH Grant P51OD011106 to the Wisconsin National Primate Research Center.

DISCLOSURES

No conflicts of interest, financial or otherwise, are declared by the authors.

AUTHOR CONTRIBUTIONS

B.K., R.D., T-Y.C., and A.R. conceived and designed research; B.K., R.D., and T-Y.C. performed experiments; Z.Z., B.K., R.D., and A.R. analyzed data; Z.Z., B.K., R.D., and A.R. interpreted results of experiments; Z.Z. and A.R. prepared figures; Z.Z. and A.R. drafted manuscript; Z.Z., B.K., R.D., T-Y.C., and A.R. edited and revised manuscript; Z.Z., B.K., R.D., T-Y.C., and A.R. approved final version of manuscript.

REFERENCES

1. **Hubel DH**, **Wiesel TN.** Sequence regularity and geometry of orientation columns in the monkey striate cortex. *J Comp Neurol* 158: 267–293, 1974. doi:10.1002/cne.901580304.
2. **Barlow HB.** Why have multiple cortical areas? *Vision Res* 26: 81–90, 1986. doi:10.1016/0042-6989(86)90072-6.
3. **Durbin R**, **Mitchison G.** A dimension reduction framework for understanding cortical maps. *Nature* 343: 644–647, 1990. doi:10.1038/343644a0.
4. **Mountcastle VB.** The columnar organization of the neocortex. *Brain* 120: 701–722, 1997. doi:10.1093/brain/120.4.701.
5. **Chklovskii DB**, **Koulakov AA.** Maps in the brain: what can we learn from them? *Annu Rev Neurosci* 27: 369–392, 2004. doi:10.1146/annurev.neuro.27.070203.144226.
6. **Issa NP**, **Rosenberg A**, **Husson TR.** Models and measurements of functional maps in V1. *J Neurophysiol* 99: 2745–2754, 2008. doi:10.1152/jn.90211.2008.
7. **Yu L**, **Yu Y.** Energy-efficient neural information processing in individual neurons and neuronal networks. *J Neurosci Res* 95: 2253–2266, 2017. doi:10.1002/jnr.24131.
8. **DeAngelis GC**, **Ghose GM**, **Ohzawa I**, **Freeman RD.** Functional micro-organization of primary visual cortex: receptive field analysis of nearby neurons. *J Neurosci* 19: 4046–4064, 1999. doi:10.1523/JNEUROSCI.19-10-04046.1999.
9. **Conway BR**, **Tsao DY.** Color-tuned neurons are spatially clustered according to color preference within alert macaque posterior inferior temporal cortex. *Proc Natl Acad Sci USA* 106: 18034–18039, 2009. doi:10.1073/pnas.0810943106.
10. **Amirikian B**, **Georgopoulos AP.** Modular organization of directionally tuned cells in the motor cortex: is there a short-range order? *Proc Natl Acad Sci USA* 100: 12474–12479, 2003. doi:10.1073/pnas.2037719100.
11. **Buneo CA**, **Andersen RA.** The posterior parietal cortex: sensorimotor interface for the planning and online control of visually guided movements. *Neuropsychologia* 44: 2594–2606, 2006. doi:10.1016/j.neuropsychologia.2005.10.011.
12. **Freedman DJ**, **Ibos G.** An integrative framework for sensory, motor, and cognitive functions of the posterior parietal cortex. *Neuron* 97: 1219–1234, 2018. doi:10.1016/j.neuron.2018.01.044.
13. **Andersen RA**, **Bracewell RM**, **Barash S**, **Gnadt JW**, **Fogassi L.** Eye position effects on visual, memory, and saccade-related activity in areas LIP and 7a of macaque. *J Neurosci* 10: 1176–1196, 1990. doi:10.1523/JNEUROSCI.10-04-01176.1990.
14. **Taira M**, **Mine S**, **Georgopoulos AP**, **Murata A**, **Sakata H.** Parietal cortex neurons of the monkey related to the visual guidance of hand movement. *Exp Brain Res* 83: 29–36, 1990. doi:10.1007/BF00232190.
15. **Duhamel JR**, **Colby CL**, **Goldberg ME.** Ventral intraparietal area of the macaque: congruent visual and somatic response properties. *J Neurophysiol* 79: 126–136, 1998. doi:10.1152/jn.1998.79.1.126.
16. **Murata A**, **Gallese V**, **Luppino G**, **Kaseda M**, **Sakata H.** Selectivity for the shape, size, and orientation of objects for grasping in neurons of monkey parietal area AIP. *J Neurophysiol* 83: 2580–2601, 2000. doi:10.1152/jn.2000.83.5.2580.
17. **Fattori P**, **Breveglieri R**, **Amoroso K**, **Galletti C.** Evidence for both reaching and grasping activity in the medial parieto-occipital cortex of the macaque. *Eur J Neurosci* 20: 2457–2466, 2004. doi:10.1111/j.1460-9568.2004.03697.x.
18. **Schlack A**, **Sterbing-D'Angelo SJ**, **Hartung K**, **Hoffmann KP**, **Bremmer F.** Multisensory space representations in the macaque ventral intraparietal area. *J Neurosci* 25: 4616–4625, 2005. doi:10.1523/JNEUROSCI.0455-05.2005.
19. **Rigotti M**, **Barak O**, **Warden MR**, **Wang XJ**, **Daw ND**, **Miller EK**, **Fusi S.** The importance of mixed selectivity in complex cognitive tasks. *Nature* 497: 585–590, 2013. doi:10.1038/nature12160.

Downloaded from journals.physiology.org/journal/jn (076.255.028.190) on April 10, 2024.

20. **Fusi S**, **Miller EK**, **Rigotti M.** Why neurons mix: high dimensionality for higher cognition. *Curr Opin Neurobiol* 37: 66–74, 2016. doi:10.1016/j.conb.2016.01.010.
21. **Vaccari FE**, **Diomedi S**, **Filippini M**, **Hadjidimitrakis K**, **Fattori P.** New insights on single-neuron selectivity in the era of population-level approaches. *Front Integr Neurosci* 16: 929052, 2022. doi:10.3389/fnint.2022.929052.
22. **Zhang T**, **Britten KH.** Clustering of selectivity for optic flow in the ventral intraparietal area. *Neuroreport* 15: 1941–1945, 2004. doi:10.1097/00001756-200408260-00022.
23. **Shao M**, **DeAngelis GC**, **Angelaki DE**, **Chen A.** Clustering of heading selectivity and perception-related activity in the ventral intraparietal area. *J Neurophysiol* 119: 1113–1126, 2018. doi:10.1152/jn.00556.2017.
24. **Rosenberg A**, **Thompson LW**, **Doudlah R**, **Chang TY.** Neuronal representations supporting three-dimensional vision in nonhuman primates. *Annu Rev Vis Sci* 9: 337–359, 2023. doi:10.1146/annurev-vision-111022-123857.
25. **Zeki S.** A direct projection from area V1 to area V3A of rhesus monkey visual cortex. *Proc R Soc Lond B Biol Sci* 207: 499–506, 1980. doi:10.1098/rspb.1980.0038.
26. **Felleman DJ**, **Van Essen DC.** Distributed hierarchical processing in the primate cerebral cortex. *Cereb Cortex* 1: 1–47, 1991. doi:10.1093/cercor/1.1.1-a.
27. **Nakamura H**, **Kuroda T**, **Wakita M**, **Kusunoki M**, **Kato A**, **Mikami A**, **Sakata H**, **Itoh K.** From three-dimensional space vision to prehensile hand movements: the lateral intraparietal area links the area V3A and the anterior intraparietal area in macaques. *J Neurosci* 21: 8174–8187, 2001. doi:10.1523/JNEUROSCI.21-20-08174.2001.
28. **Taira M**, **Tsutsui KI**, **Jiang M**, **Yara K**, **Sakata H.** Parietal neurons represent surface orientation from the gradient of binocular disparity. *J Neurophysiol* 83: 3140–3146, 2000. doi:10.1152/jn.2000.83.5.3140.
29. **Tsutsui K**, **Sakata H**, **Naganuma T**, **Taira M.** Neural correlates for perception of 3D surface orientation from texture gradient. *Science* 298: 409–412, 2002. doi:10.1126/science.1074128.
30. **Tsao DY**, **Vanduffel W**, **Sasaki Y**, **Fize D**, **Knutsen TA**, **Mandeville JB**, **Wald LL**, **Dale AM**, **Rosen BR**, **Van Essen DC**, **Livingstone MS**, **Orban GA**, **Tootell RB.** Stereopsis activates V3A and caudal intraparietal areas in macaques and humans. *Neuron* 39: 555–568, 2003. doi:10.1016/s0896-6273(03)00459-8.
31. **Tsutsui K**, **Jiang M**, **Sakata H**, **Taira M.** Short-term memory and perceptual decision for three-dimensional visual features in the caudal intraparietal sulcus (area CIP). *J Neurosci* 23: 5486–5495, 2003. doi:10.1523/JNEUROSCI.23-13-05486.2003.
32. **Rosenberg A**, **Cowan NJ**, **Angelaki DE.** The visual representation of 3D object orientation in parietal cortex. *J Neurosci* 33: 19352–19361, 2013. doi:10.1523/JNEUROSCI.3174-13.2013.
33. **Rosenberg A**, **Angelaki DE.** Reliability-dependent contributions of visual orientation cues in parietal cortex. *Proc Natl Acad Sci USA* 111: 18043–18048, 2014. doi:10.1073/pnas.1421131111.
34. **Elmore LC**, **Rosenberg A**, **DeAngelis GC**, **Angelaki DE.** Choice-related activity during visual slant discrimination in macaque CIP but not V3A. *eNeuro* 6: ENEURO.0248-18.2019, 2019. doi:10.1523/ENEURO.0248-18.2019.
35. **Chang TY**, **Doudlah R**, **Kim B**, **Sunkara A**, **Thompson LW**, **Lowe ME**, **Rosenberg A.** Functional links between sensory representations, choice activity, and sensorimotor associations in parietal cortex. *Elife* 9: e57968, 2020. doi:10.7554/eLife.57968.
36. **Doudlah R**, **Chang TY**, **Thompson LW**, **Kim B**, **Sunkara A**, **Rosenberg A.** Parallel processing, hierarchical transformations, and sensorimotor associations along the 'where' pathway. *Elife* 11: e78712, 2022. doi:10.7554/eLife.78712.
37. **Galletti C**, **Battaglini PP.** Gaze-dependent visual neurons in area V3A of monkey prestriate cortex. *J Neurosci* 9: 1112–1125, 1989. doi:10.1523/JNEUROSCI.09-04-01112.1989.
38. **Galletti C**, **Battaglini PP**, **Fattori P.** 'Real-motion' cells in area V3A of macaque visual cortex. *Exp Brain Res* 82: 67–76, 1990. doi:10.1007/BF00230838.
39. **Sauvan XM**, **Peterhans E.** Orientation constancy in neurons of monkey visual cortex. *Vis Cogn* 6: 43–54, 1999. doi:10.1080/713756803.
40. **Nakamura K**, **Colby CL.** Visual, saccade-related, and cognitive activation of single neurons in monkey extrastriate area V3A. *J Neurophysiol* 84: 677–692, 2000. doi:10.1152/jn.2000.84.2.677.
41. **Nakamura K**, **Colby CL.** Updating of the visual representation in monkey striate and extrastriate cortex during saccades. *Proc Natl Acad Sci USA* 99: 4026–4031, 2002. doi:10.1073/pnas.052379899.
42. **Rosenberg A**, **Angelaki DE.** Gravity influences the visual representation of object tilt in parietal cortex. *J Neurosci* 34: 14170–14180, 2014. doi:10.1523/JNEUROSCI.2030-14.2014.
43. **Sakata H**, **Taira M**, **Kusunoki M**, **Murata A**, **Tanaka Y**, **Tsutsui K.** Neural coding of 3D features of objects for hand action in the parietal cortex of the monkey. *Philos Trans R Soc Lond B Biol Sci* 353: 1363–1373, 1998. doi:10.1098/rstb.1998.0290.
44. **Premereur E**, **Van Dromme IC**, **Romero MC**, **Vanduffel W**, **Janssen P.** Effective connectivity of depth-structure-selective patches in the lateral bank of the macaque intraparietal sulcus. *PLoS Biol* 13: e1002072, 2015. doi:10.1371/journal.pbio.1002072.
45. **Van Dromme IC**, **Premereur E**, **Verhoef BE**, **Vanduffel W**, **Janssen P.** Posterior parietal cortex drives inferotemporal activations during three-dimensional object vision. *PLoS Biol* 14: e1002445, 2016. doi:10.1371/journal.pbio.1002445.
46. **Lanzilotto M**, **Ferroni CG**, **Livi A**, **Gerbella M**, **Maranesi M**, **Borra E**, **Passarelli L**, **Gamberini M**, **Fogassi L**, **Bonini L**, **Orban GA.** Anterior intraparietal area: a hub in the observed manipulative action network. *Cereb Cortex* 29: 1816–1833, 2019. [Erratum in Cereb Cortex 30: 100, 2020]. doi:10.1093/cercor/bhz011.
47. **Chang TY**, **Thompson L**, **Doudlah R**, **Kim B**, **Sunkara A**, **Rosenberg A.** Optimized but not maximized cue integration for 3D visual perception. *eNeuro* 7: ENEURO.0411-19.2019, 2020. doi:10.1523/ENEURO.0411-19.2019.
48. **Munoz DP**, **Wurtz RH.** Saccade-related activity in monkey superior colliculus. I. Characteristics of burst and buildup cells. *J Neurophysiol* 73: 2313–2333, 1995. doi:10.1152/jn.1995.73.6.2313.
49. **Hanes DP**, **Schall JD.** Neural control of voluntary movement initiation. *Science* 274: 427–430, 1996. doi:10.1126/science.274.5286.427.
50. **Kim B**, **Kenchappa SC**, **Sunkara A**, **Chang TY**, **Thompson L**, **Doudlah R**, **Rosenberg A.** Real-time experimental control using network-based parallel processing. *Elife* 8: e40231, 2019. doi:10.7554/eLife.40231.
51. **Stevens KA.** Slant-tilt: the visual encoding of surface orientation. *Biol Cybern* 46: 183–195, 1983. doi:10.1007/BF00336800.
52. **Gray CM**, **Maldonado PE**, **Wilson M**, **McNaughton B.** Tetrodes markedly improve the reliability and yield of multiple single-unit isolation from multi-unit recordings in cat striate cortex. *J Neurosci Methods* 63: 43–54, 1995. doi:10.1016/0165-0270(95)00085-2.
53. **Bingham C.** An antipodally symmetric distribution on the sphere. *Ann Stat* 2: 1201–1225, 1974. doi:10.1214/aos/1176342874.
54. **Prince SJ**, **Pointon AD**, **Cumming BG**, **Parker AJ.** Quantitative analysis of the responses of V1 neurons to horizontal disparity in dynamic random-dot stereograms. *J Neurophysiol* 87: 191–208, 2002. doi:10.1152/jn.00465.2000.
55. **Alme CB**, **Miao C**, **Jezek K**, **Treves A**, **Moser EI**, **Moser MB.** Place cells in the hippocampus: Eleven maps for eleven rooms. *Proc Natl Acad Sci USA* 111: 18428–18435, 2014. doi:10.1073/pnas.1421056111.
56. **Matelli M**, **Luppino G.** Parietofrontal circuits for action and space perception in the macaque monkey. *Neuroimage* 14: S27–32, 2001. doi:10.1006/nimg.2001.0835.
57. **Grefkes C**, **Ritzl A**, **Zilles K**, **Fink GR.** Human medial intraparietal cortex subserves visuomotor coordinate transformation. *Neuroimage* 23: 1494–1506, 2004. doi:10.1016/j.neuroimage.2004.08.031.
58. **Creem-Regehr SH.** Sensory-motor and cognitive functions of the human posterior parietal cortex involved in manual actions. *Neurobiol Learn Mem* 91: 166–171, 2009. doi:10.1016/j.nlm.2008.10.004.
59. **Goard MJ**, **Pho GN**, **Woodson J**, **Sur M.** Distinct roles of visual, parietal, and frontal motor cortices in memory-guided sensorimotor decisions. *Elife* 5: e13764, 2016. doi:10.7554/eLife.13764.
60. **Pho GN**, **Goard MJ**, **Woodson J**, **Crawford B**, **Sur M.** Task-dependent representations of stimulus and choice in mouse parietal cortex. *Nat Commun* 9: 2596, 2018. [Erratum in Nat Commun 10: 389, 2019]. doi:10.1038/s41467-018-05012-y.
61. **Shushruth S**, **Mazurek M**, **Shadlen MN.** Comparison of decision-related signals in sensory and motor preparatory responses of neurons in area LIP. *J Neurosci* 38: 6350–6365, 2018. doi:10.1523/JNEUROSCI.0668-18.2018.

Downloaded from journals.physiology.org/journal/jn (076.255.028.190) on April 10, 2024.

62. **Zhou Y**, **Freedman DJ.** Posterior parietal cortex plays a causal role in perceptual and categorical decisions. *Science* 365: 180–185, 2019. doi:10.1126/science.aaw8347.
63. **Zhang Z**, **Yin C**, **Yang T.** Evidence accumulation occurs locally in the parietal cortex. *Nat Commun* 13: 4426, 2022. doi:10.1038/s41467-022-32210-6.
64. **Eskandar EN**, **Assad JA.** Dissociation of visual, motor and predictive signals in parietal cortex during visual guidance. *Nat Neurosci* 2: 88–93, 1999. doi:10.1038/4594.
65. **McGuire LM**, **Sabes PN.** Heterogeneous representations in the superior parietal lobule are common across reaches to visual and proprioceptive targets. *J Neurosci* 31: 6661–6673, 2011. doi:10.1523/JNEUROSCI.2921-10.2011.
66. **Avillac M**, **Ben Hamed S**, **Duhamel JR.** Multisensory integration in the ventral intraparietal area of the macaque monkey. *J Neurosci* 27: 1922–1932, 2007. doi:10.1523/JNEUROSCI.2646-06.2007.
67. **Sunkara A**, **DeAngelis GC**, **Angelaki DE.** Role of visual and non-visual cues in constructing a rotation-invariant representation of heading in parietal cortex. *Elife* 4: e04693, 2015. doi:10.7554/eLife.04693.
68. **Tsutsui K**, **Jiang M**, **Yara K**, **Sakata H**, **Taira M.** Integration of perspective and disparity cues in surface-orientation-selective neurons of area CIP. *J Neurophysiol* 86: 2856–2867, 2001. doi:10.1152/jn.2001.86.6.2856.
69. **Murasugi CM**, **Salzman CD**, **Newsome WT.** Microstimulation in visual area MT: effects of varying pulse amplitude and frequency. *J Neurosci* 13: 1719–1729, 1993. doi:10.1523/JNEUROSCI.13-04-01719.1993.

Downloaded from journals.physiology.org/journal/jn (076.255.028.190) on April 10, 2024.